Global J. Environ. Sci. Manage. 7(4): 485-502, Autumn 2021

Global Journal of Environmental Science and Management
(GJESM)

Homepage: https://www.gjesm.net/

ORIGINAL RESEARCH PAPER

Application of amorphous zirconium (hydr)oxide/MgFe layered double hydroxides composite in fixed-bed column for phosphate removal from water

A. Nuryadin[1,2], T. Imai[1,*]

[1]*Graduate School of Sciences and Technology for Innovation, Yamaguchi University, Yamaguchi, 755-8611, Japan*

[2]*Department of Physics Education, Mulawarman University, Samarinda, 75123, Indonesia*

ARTICLE INFO

Article History:
Received 04 January 2021
Revised 02 March 2021
Accepted 11 April 2021

Keywords:
Adsorbent regeneration
Amorphous zirconia
Fixed-bed column
Layered double hydroxides
Phosphate adsorption
Phosphate adsorption mechanism

ABSTRACT

BACKGROUND AND OBJECTIVES: Fixed-bed column has been considered an industrially feasible technique for phosphate removal from water. Besides the adsorption capacity, the effectiveness of an adsorbent is also determined by its reusability efficiency. In this study, phosphate removal by a synthesized amorphous zirconium (hydr)oxide/MgFe layered double hydroxides composite in a fixed-bed column system was examined.

METHODS: The effects of flow rate, bed height, phosphate concentration, solution pH, and adsorbent particle size on the phosphate adsorption ability were examined through a series of continuous adsorption experiments. The appropriate breakthrough curve models, phosphate adsorption from real anaerobic sludge and synthetic seawater, column regeneration and reusability, and adsorption mechanism were also investigated for practical application feasibility.

FINDINGS: The results showed that the increased bed height and phosphate concentration, and reduced flow rate, pH, and adsorbent particle size were found to increase the column adsorption capacity. The optimum adsorption capacity of 25.15 mg-P/g was obtained at pH 4. The coexistence of seawater ions had a positive effect on the phosphate adsorption capacity of the composite. Nearly complete phosphate desorption, with a desorption efficiency of 91.7%, could be effectively achieved by 0.1 N NaOH for an hour. Moreover, the initial adsorption capacity was maintained at approximately 83% even after eight adsorption-desorption cycles, indicating that the composite is economically feasible. The high phosphate adsorption capacity of the composite involves three main adsorption mechanisms, which are electrostatic attraction, inner-sphere complexation, and anion exchange, where the amorphous zirconium hydr(oxide) on the surface of the layered double hydroxides likely increased the number of active binding sites and surface area for adsorption.

CONCLUSION: The amorphous zirconium (hydr)oxide/MgFe layered double hydroxides composite, with its high adsorption capacity and superior reusability, has the potential to be utilized as an adsorbent for phosphorus removal in practical wastewater treatment. This study provides insights into the design of amorphous zirconium (hydr)oxide/MgFe layered double hydroxides composite for phosphorus removal and recovery in a practical system.

DOI: 10.22034/gjesm.2021.04.01

NUMBER OF REFERENCES	NUMBER OF FIGURES	NUMBER OF TABLES
39	9	4

*Corresponding Author:
Email: *imai@yamaguchi-u.ac.jp*
Phone: +81-836-85-9300
Fax: +81-836-85-9301

Note: Discussion period for this manuscript open until January 1, 2022 on GJESM website at the "Show Article.

INTRODUCTION

Phosphates are vital for the sustainability of organisms and several industrial activities. However, their widespread use, along with the increase in population, has induced superfluous levels of phosphates in the aquatic environment, leading to water eutrophication (Dash *et al.*, 2020). Thus, it is essential to minimize or eliminate phosphorus contaminations from wastewater prior to its discharge into the receiving water body to maintain water quality and improve human health. Additionally, the global increase in food demand and limited carrying capacity of land has increased the dependence on phosphorus, which is used to increase agricultural productivity to fulfill human and livestock needs (March *et al.*, 2016). As phosphorus is a non-renewable natural resource and cannot be substituted by other resources (Wang *et al.*, 2021), the recovery of phosphates from wastewater is important for the sustainability of global phosphorus reserves.

In the last decade, numerous phosphate removal techniques have been designed, ranging from adsorption and chemical precipitation to the application of polyphosphate-accumulating organisms (PAOs) (Ramasahayam *et al.*, 2014). Among these techniques, adsorption is constantly gaining popularity owing to its simplicity and the possibility of phosphorus recovery from wastewater (Zou *et al.*, 2020). However, the cost-effectiveness depends on the reusability of the adsorbent (Kumar *et al.*, 2019). Consequently, adsorbents with high chemical stability are being preferred for phosphorus adsorption because of their stability during the desorption process under various stripping agent chemistry conditions, which usually use a solution with extreme acidity or alkalinity.

Nuryadin *et al.* (2021) synthesized a composite of amorphous zirconium (hydr)oxide/MgFe layered double hydroxides (am-Zr/MgFe-LDH) using a novel two-stage synthesis. A series of batch experiments showed that the uncalcined am-Zr/MgFe-LDH composite with a Zr:Fe ratio of 1:5 showed a high adsorption performance towards phosphates and retained good removal efficiency over eight adsorption-desorption cycles. The high adsorption capacity is related to the high surface area and large number of hydroxyl groups on the composite as a consequence of small crystal size and low agglomeration of amorphous zirconium (hydr)oxide (am-Zr) in the composite. However, batch settings are not suitable for large-scale applications and continuously generated wastewater (Taka *et al.*, 2020). Therefore, it is important to understand the application of the composite in continuous fixed-bed column adsorption to investigate its performance in practical applications. Fixed-bed column adsorption is very popular in wastewater treatment because of its continuous, high yield, simple, and economical operation and the ability to be scaled-up from the laboratory-scale (Jiang *et al.*, 2018; Kumar *et al.*, 2011). Sun *et al.* (2014) found that MgFe-LDH in a fixed-bed column had a high phosphate adsorption capacity and acceptable desorption efficiency. However, no studies have been conducted on the phosphate removal performance of the am-Zr/MgFe-LDH composite in a fixed-bed column.

In this study, the effects of design parameters essential for practical applications, such as flow rate, bed height, influent phosphate concentration, pH, and adsorbent particle size on the am-Zr/MgFe-LDH composite performance for phosphate removal were examined. Furthermore, the three most widely used models, Thomas, Yoon-Nelson, and modified dose-response (MDR) models were applied to interpret the phosphate adsorption breakthrough data. The applicability of the composite for real anaerobic sludge and phosphate-enriched seawater and its reusability were also evaluated. In addition, an adsorption mechanism of phosphate on the composite was proposed for designing a practical system for the removal and recovery of phosphorus. The objective of the current study is to investigate the phosphate adsorption performance and reusability of a fixed-bed column filled with the am-Zr/MgFe-LDH composite. This study has been carried out in Environmental Planning Laboratory, Graduate School of Sciences and Technology for Innovation, Yamaguchi University, Ube, Japan during 2018-2020.

MATERIALS AND METHODS

Adsorbent and adsorbate preparation

Analytical grade $FeCl_3 \cdot 6H_2O$ (99.0% pure), $MgCl_2 \cdot 6H_2O$ (98.0% pure), $ZrOCl_2 \cdot 8H_2O$ (99.0% pure), Na_2CO_3 (99.8% pure), NaOH (97.0% pure) were purchased from Wako Pure Chemical Industries, Ltd. for preparing the am-Zr/MgFe-LDH composite, and used directly in this study without further purification.

A composite with a Zr:Fe molar ratio of 1.5:1 was synthesized using an established method (Nuryadin *et al*., 2021). Briefly, a solution containing Mg^{2+} and Fe^{3+} ions with a molar ratio of 3:1 was poured into 200 mL of deionized (DI) water. The solution pH was maintained at ~10 using a solution of 1 M NaOH and 1 M Na_2CO_3 with a 3:1 volume ratio under vigorous stirring for 30 min. The separated and neutralized gel obtained was then mixed with $ZrOCl_2{\cdot}8H_2O$ (Zr to Fe molar ratio of 1.5:1) in 500 mL of DI water. Simultaneously, a 25% NaOH solution was used to precipitate the am-Zr under constant stirring until a pH of ~10 was obtained. After aging at 353 K for 24 h, the composite was filtered, washed with DI water for neutralization, and then dried in an oven at 353 K for 24 h. The dried composite was ground in a mortar and sieved to the desired particle size.

K_2HPO_4 (99.0% pure) was obtained from Wako Pure Chemical Industries, Ltd., Japan. A phosphate stock solution (500 mg-P/L) was prepared by dissolving an appropriate amount of K_2HPO_4 in 1 L of DI water. The stock solution was diluted to the desired working solution using DI water. The pH of the working solution was adjusted using 0.1 M HCl and NaOH solutions and monitored using a pH meter (Horiba, LAQUA SS131 D-71).

Adsorbent characterization

The X-ray diffraction (XRD) pattern of the adsorbent, with particle size of $d \leq 0.1$ mm, was recorded on a Rigaku Ultima IV Protectus diffractometer using Cu-Kα radiation at 40 kV. Fourier transform infrared (FTIR) spectra of the composites before and after adsorption were recorded on a Jasco FT/IR-4600 spectrophotometer. The X-ray photoelectron spectroscopy (XPS) spectra were obtained using a Thermo Scientific K-alpha X-ray photoelectron spectrometer and fitted with XPSPEAK41 and Origin 9.4 software. The high-resolution scans of XPS focused on Mg, Fe, Zr, C, and O. The pH at the point of zero charge (pH_{pzc}) of the composite was investigated using potentiometric mass titration (PMT), as described by Bourikas *et al*. (2003). Three different doses of the composite (5, 15, and 25 g/L) were immersed in Erlenmeyer flasks containing 100 mL of 0.03 M KNO_3 and shaken under an N_2 atmosphere at 200 rpm for 24 h. In each flask, 0.5 mL of 1 M KOH was added to deprotonate sites in the composite surface, and the shaken samples were titrated using a 0.1 M HNO_3 solution. The titration curve was constructed by plotting the pH value as a function of HNO_3 volume.

Adsorption experiment

Continuous fixed-bed column adsorption experiments were conducted at room temperature (~298 K) using a non-jacketed liquid chromatography column (Sigma-Aldrich, Co.) with an inner diameter of 1.0 cm and a length of 10 cm. Fig. 1 shows a schematic diagram of the fixed-bed column system used in this study. A 1 cm thick glass wool was placed on the top and bottom of the sample to prevent the adsorbent from being washed out by the liquid flow. A particular weight (0.7, 1.0, and 1.4 g) of the composite with a maximum particle size of 106 µm was packed into the column to attain the desired bed height (h) (1.0, 1.5, and 2.0 cm). The artificial influent phosphate solution with various concentrations (C_o) (5 mg-P/L, 12 mg-P/L, and 20 mg-P/L) at pH 7 was pumped in an up-flow configuration through the packed composite inside the column at varying flow rates (Q) (1.5, 2.5, and 3.5 mL/min) using a peristaltic pump (EYELA MP-1000). The effects of phosphate solution pH (4, 7, and 10) and composite particle size (d) (≤ 0.1, 0.1–0.5, and 0.5–1.0 mm) on phosphate adsorption were examined. To obtain the breakthrough curves, the effluent solutions were automatically collected at specified intervals using a fraction collector (Advantec SF-3120) for measuring phosphate concentrations. In this study, the breakthrough time was assigned when the ratio of effluent to influent phosphate concentration (C/Co) was 10%. An exhaustion time is the time when the influent solution passes through the adsorbent without any significant decrease in concentration (Marzbali and Esmaieli, 2017). A preliminary experiment showed that the breakthrough curves became relatively flat after C/Co reached approximately 85% and the phosphate adsorption became insignificant. Therefore, the exhaustion time in this study was determined to be the time when C/Co reached 85%.

Breakthrough curves of phosphate adsorption were constructed by plotting the ratio of effluent phosphate concentration at an interval time to influent phosphate concentration (C/Co) as a function of time (t). The breakthrough curves demonstrate the mass transfer characteristics of phosphate onto the

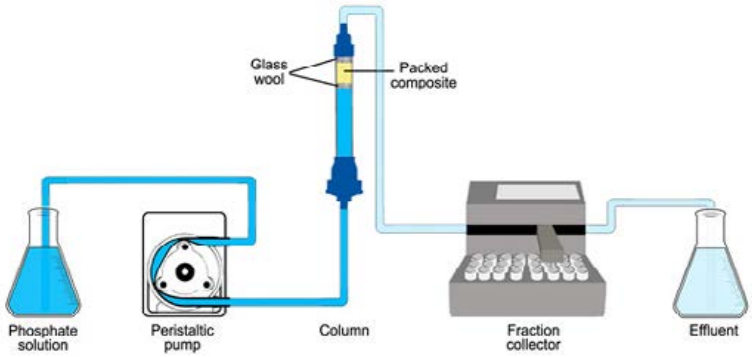


Fig. 1: Schematic diagram of lab-scale fixed-bed column adsorption system

packed composite. The total amount of adsorbed phosphate, $q_{adsorbed}$ (mg), during adsorption and the equilibrium adsorption capacity, q_e (mg/g), were calculated as follows (Eqs. 1 and 2, respectively) (Gouran-Orimi *et al*., 2018).

$$q_{adsorbed} = \frac{QC_0}{1000}\int_{t=0}^{t=t_e}\left(1-\frac{C}{C_0}\right)dt \quad (1)$$

$$q_e = \frac{q_{adsorbed}}{m} \quad (2)$$

Where, Q is the flow rate (mL/min), C_0 and C are the influent and effluent phosphate concentrations (mg/L), respectively, t_e is the time required to reach exhaustion time (min), and m is the weight of the composite packed inside the column (g).

Regeneration and reusability experiment

Before the regeneration experiment, the exhausted bed in the column was washed with DI water at a flow rate of 2.5 mL/min for 1 h to remove residual phosphorus. Subsequently, 0.1 M NaOH was pumped in the opposite direction to desorb the adsorbed phosphate. In this study, regeneration was done until the effluent concentration reached approximately 0.5 mg-P/L and it was assumed that the column had been regenerated. In the first cycle of desorption, the desorption effluent solutions were collected at the pre-determined intervals to obtain the desorption curve. The amount of phosphorus eluted from the composite (EAP) (mg/g) was calculated using the following equations (Eqs. 3 and 4) (Nguyen *et al*., 2015):

$$EAP = \frac{1}{m}q_{desorbed} \quad 3)$$

$$q_{desorbed} = \sum_{q=1}^{n2} CV_q \quad (4)$$

Where, m is the weight of adsorbent in the column (g), $q_{desorbed}$ is the total amount of desorbed phosphate (mg), V_q is the effluent volume of the q -th fraction (L), and $n2$ is the number of the last fraction in the desorption operation. Desorption and regeneration experiments were conducted for eight cycles of the adsorption-desorption process.

RESULTS AND DISCUSSION

Fixed-bed column adsorption studies

The effect of phosphate solution flow rate on the phosphate adsorption on the composite in the column was investigated at three different flow rates (1.5, 2.5, and 3.5 mL/min), where the bed height (1.5 cm) and the influent phosphate concentration (12 mg-P/L) were kept constant. Fig. 2a shows the effect of the flow rate on the breakthrough curve of phosphate adsorption on the composite. The increase in flow rate from 1.5 to 3.5 mL/min resulted in reduction in the breakthrough time from 14.9 to 5.5 h and in the exhaustion time from 24.0 to 8.9 h. The increase in the flow rate led to an increase in the volume speed, leading to a reduction in the time required to reach breakthrough and exhaustion states. The adsorption capacity, calculated using Eq. 2, decreased from 20.40 to 18.23 mg-P/g as the flow rate increased from 1.5 to 3.5 mL/min (Table 1). At a high flow rate, the phosphate anions have a short

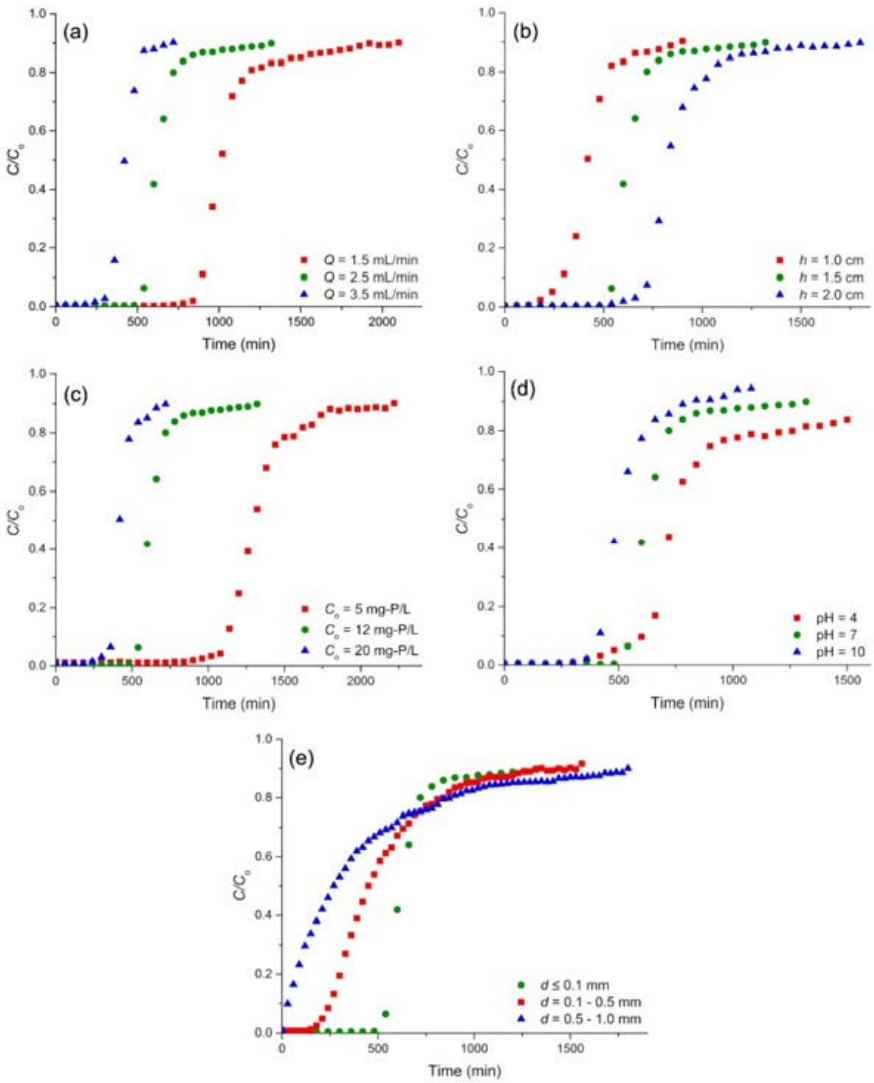


Fig. 2: The Effect of (a) flow rate (h = 1.5 cm, C_o = 12 mg-P/L, pH = 7, and $d \leq 0.1$ mm), (b) bed height (Q = 2.5 mL/min, C_o = 12 mg-P/L, pH = 7, and $d \leq 0.1$ mm), (c) influent phosphate concentration (h = 1.5 cm, Q = 2.5 mL/min, pH = 7, and $d \leq 0.1$ mm), (d) solution pH (h = 1.5 cm, Q = 2.5 mL/min, C_o = 12 mg-P/L, and $d \leq 0.1$ mm), and (e) composite particle size (m = 1.01 g cm, Q = 2.5 mL/min, C_o = 12 mg-P/L, and pH = 7), on the fixed-bed column studies

residence time in the bed, where composite particles in the fixed-bed column have a short contact time with the phosphate anions as the solution flows through the bed (Gouran-Orimi *et al.*, 2018). Consequently, the possibility of phosphate anions passing through the column before being completely adsorbed increased because of the insufficient contact time for adsorption equilibrium. In addition, the steepness of the breakthrough curves increased with the increase in flow rate. The different slope of the breakthrough curves was due to the retention process. A high flow rate led to an increase in mass transfer rate, increasing the amount of phosphate captured onto the adsorbent surface in the beginning of operation. This caused an early saturation with a steeper slope given in the breakthrough curves.

Breakthrough curves resulting from fixed-bed column experiments at different bed heights (1.0, 1.5, and 2.0 cm) with a constant flow rate (2.5 mL/min) and influent phosphate concentration (12 mg-

Table 1: Fixed-bed column parameters for phosphate adsorption on am-Zr/MgFe-LDH composite

No..	Q (mL/min)	h (cm)	C_o (mg-P/L)	m (g)	pH	d (mm)	t_b (h)	τ (h)	t_e (h)	q_e (mg-P/g)
1	1.5	1.5	12	1.01	7	≤ 0.1	14.9	17.33	24.0	20.40
2	2.5	1.5	12	1.01	7	≤ 0.1	9.1	10.65	13.5	19.04
3	3.5	1.5	12	1.01	7	≤ 0.1	5.5	7.19	8.9	18.23
4	2.5	1.0	12	0.68	7	≤ 0.1	4.8	7.24	10.7	18.75
	2.5	1.5	12	1.01	7	≤ 0.1	9.1	10.65	13.5	19.04
5	2.5	2.0	12	1.36	7	≤ 0.1	12.1	14.48	19.0	19.56
6	2.5	1.5	5	1.01	7	≤ 0.1	18.7	22.28	28.7	17.08
	2.5	1.5	12	1.01	7	≤ 0.1	9.1	10.65	13.5	19.04
7	2.5	1.5	20	1.01	7	≤ 0.1	4.4	6.04	7.8	19.13
8	2.5	1.5	12	1.01	4	≤ 0.1	10.0	12.82	25.0	25.15
	2.5	1.5	12	1.01	7	≤ 0.1	9.1	10.65	13.5	19.04
9	2.5	1.5	12	1.01	10	≤ 0.1	6.9	8.63	11.5	15.73
	2.5	1.5	12	1.01	7	≤ 0.1	9.1	10.65	13.5	19.04
10	2.5	1.8	12	1.01	7	0.1–0.5	4.2	7.51	16.0	15.80
11	2.5	2.0	12	1.01	7	0.5–1	0.5	4.49	19.0	12.45

P/L) are depicted in Fig. 2b. The figure demonstrates that the breakthrough and exhaustion times were extended when the bed height increased. Table 1 shows that the adsorption capacity increased from 18.75 to 19.56 mg-P/g as the bed height increased from 1.0 to 2.0 cm. This was predictable as there were more active binding sites at a higher bed height, and these increased the adsorption areas (Mohan and Dutta, 2020). Furthermore, a higher bed height provides a longer packed composite through which the phosphate anions pass, which allows a longer residence time of phosphate, enabling it to be deeply adsorbed within the composite. The bed height of 2.0 cm had a flatter breakthrough curve than the lower bed height, which might be due to a broad mass transfer zone provided by a high bed height.

Fig. 2c shows the adsorption curves of various influent phosphate concentrations (5, 12, and 20 mg-P/L) at a constant bed height (1.5 cm) and flow rate (2.5 mL/min). An increase in influent phosphate concentration from 5 to 20 mg-P/L decreased the breakthrough time from 18.7 to 4.4 h and exhaustion time from 28.7 to 7.8 h. The concentration gradient between the solution and adsorbent surface increased at high phosphate concentrations, which increased the driving force for phosphate adsorption (Lee *et al*., 2019). Under these conditions, the limited active binding sites in the column were inhibited rapidly, and saturated conditions were achieved in a short period. This led to a steeper breakthrough curve at higher influent phosphate concentrations. This steeper curve at the high load of phosphate anions signifies that the am-Zr/MgFe-LDH is likely favorable for phosphate adsorption. The adsorption capacity increased from 17.08 to 19.13 mg-P/g when the influent phosphate concentration was raised from 5 to 20 mg-P/L. A higher influent concentration of phosphate can deliver more phosphate anions into the outer and inner surface of the composite to attach with the adsorption sites, which is possibly the reason for an increase in adsorption capacity with influent concentration increasing. In addition, a high concentration gradient at high influent phosphate concentration can overcome the mass transfer resistance in the adsorbent surface, leading to an increase in the adsorption capacity.

Another important parameter that affects the dynamic phosphate adsorption process in a fixed-bed column is the pH solution. Fig. 2d shows the effect of phosphate solution pH (4, 7, and 10) on phosphate adsorption breakthrough curves, while maintaining a constant bed height (1.5 cm), flow rate (2.5 mL/min), and influent phosphate concentration (12 mg-P/L). It can be seen clearly that the breakthrough time was reached in a longer time at a lower pH. The breakthrough time increased from 6.9 to 10.0

h with decreasing pH from 10 to 4. As shown in Table 1, a higher adsorption capacity (25.15 mg-P/g) was obtained at a lower pH (acidic solution). The adsorption capacity decreased significantly when the influent pH increased from 4 to 10, signifying that pH played a key role which affected the physical-chemical interaction between the phosphate and composite surface. The adsorbent surface was positively charged at low pH, attracting the negatively charged phosphate anions. Conversely, the number of hydroxyl ions (OH^-) increased at higher pH, which competed with phosphate anions to occupy more active binding sites on the adsorbent surface and led to the reduction of phosphate adsorption onto the composite surface (He *et al*., 2016). The lower pH showed a broader tailing edge in the breakthrough curve shape, reflecting that the phosphate adsorption onto composite bed in lower pH was extended with a slow adsorption.

The effect of composite particle size on the breakthrough curve of phosphate adsorption was investigated by isolating the composite into three groups of particle sizes using sieves with apertures of different sizes (≤ 0.1 mm, 0.1–0.5 mm, and 0.5–1.0 mm). The bed height (1.5 cm), flow rate (2.5 mL/min), and influent phosphate concentration (12 mg-P/L) were kept constant. Fig. 2e shows the breakthrough curves of phosphate adsorption resulting from different composite particle sizes. The bed performance of the smallest particle size (≤ 0.1 mm) was better than that of the larger particle sizes, particularly for the initial part of the curve. The reduction in particle size led to a longer breakthrough time but a shorter exhaustion time. As the particle size of the composite increased, the surface area per unit volume decreased. Consequently, the number of active binding sites on the surface of composite with large particle size, that directly interact with the phosphate ions in the solution, smaller than the composite with a lower particle size resulted in an earlier breakthrough time corresponding to the completion of surface adsorption. However, after the breakthrough point was achieved in the large particle composite, the pore adsorption continued at a lower rate, which resulted in a delayed exhaustion time. Additionally, for smaller particle sizes with a higher surface area (Oguz, 2017), phosphate adsorption mostly occurred on the surface of the composite with a large number of exposed active binding sites. A decrease in particle size appears to have increased the sharpness of the breakthrough curves and delayed the breakthrough time.

Table 2 summarizes the phosphate adsorption capacity of am-Zr/MgFe-LDH composite in this study and calcined MgFe-LDH as well as other Zr-based adsorbents in fixed-bed column adsorption. It was demonstrated that am-Zr/MgFe-LDH composite was found to have higher adsorption capacity than calcined MgFe-LDH and positively comparable to most of the Zr-based adsorbents reported in the literature. This result confirmed that the combination of am-Zr and MgFe-LDH resulted in favorable modification in the adsorbent surface for effective phosphate adsorption. The high phosphate adsorption capacity of am-Zr/MgFe-LDH composite can be associated with the development of a high amount of hydroxyl groups in the adsorbent surface by am-Zr, where the hydroxyl groups act as the effective binding sites for phosphate anions.

Breakthrough curve modeling

Generally, the modeling of breakthrough curves

Table 2: Comparison of the phosphate adsorption capacity of am-Zr/MgFe-LDH composite with various adsorbents in fixed-bed column

Adsorbent	Experimental condition					q_e (mg-P/g)	Reference
	Q (mL/min)	h (cm)	C_o (mg-P/L)	pH	d (mm)		
Zr-FPS	1.77	1.6	0.411	2.01	-	1.73	Awual *et al*., 2011
Zirconium ferrite	0.083	-	20	7	0.7	2.6	Biswas *et al*., 2008
A-Zr-NP	6	4.8	20	5.4	-	5.59	Husein *et al*., 2017
Zr(IV)-loaded SOW gel	0.083	-	20	7	0.075–0.15	10	Biswas *et al*., 2008
Zr(IV)-loaded okara	12	9	5.5	7.6	0.3–0.15	14.97	Nguyen *et al*., 2015
Zr(IV)-loaded okara	12	23	5.6	3	1–0.6	16.43	Nguyen *et al*., 2015
Calcined MgFe-LDH	0.4	12	20	-	0.075–0.028	21.09	Sun *et al*., 2014
CS-Zr-PEPA	6	12	2.4	6.5	-	32.50	Chen *et al*., 2020
Am-Zr/MgFe-LDH	2.5	1.5	12	4	≤ 0.1	25.15	Present study

resulting from fixed-bed column adsorption is essential for designing a column adsorption system for practical applications. To describe the behavior of dynamic phosphate adsorption onto the am-Zr/MgFe-LDH composite in a fixed-bed column system, three nonlinear mathematical model equations, Yoon-Nelson (Eq. 5) (Yoon and Nelson, 1984), Thomas (Eq. 6) (Thomas, 1944), and MDR models (Eq. 7) (Yan *et al*., 2001) were used.

$$\ln\left(\frac{C}{C_o - C}\right) = k_{YN}t - \tau k_{YN} \quad (5)$$

$$\ln\left(\frac{C_o}{C} - 1\right) = \frac{k_{Th}q_{Th}m}{Q} - k_{Th}C_o t \quad (6)$$

$$\ln\left(\frac{C}{C_0 - C}\right) = a\ln\left(\frac{C_o Qt}{1000}\right) - a\ln q_{mdr}m \quad (7)$$

Where, k_{Th} and k_{YN} are the Thomas kinetic coefficient (L/mg min) and the Yoon-Nelson kinetic coefficient (1/min), respectively, q_{Th} and q_{mdr} are the predicted adsorption capacities (mg/g), τ is the time required for 50% phosphate adsorption breakthrough (min), and a is an MDR model parameter.

The main parameters of each mathematical model obtained by non-linear fitting of the breakthrough data under different experimental conditions are presented in Table 3. A simple Yoon-Nelson model was applied to examine the phosphate adsorption behavior of the packed composite. This model assumes that the decrease in the adsorption probability of each molecule is proportional to the adsorption probability of the molecule and the probability of molecule breakthrough on the adsorbent (Sotelo *et al*., 2012). Although this model is based on the adsorption probability, the R^2 (0.864–0.984) values showed a good fit with the experimental data. Additionally, the predicted values of τ were similar to those obtained from experiments (Table 1), except for d values of 0.1–0.5 and 0.5–1.0 nm, where the breakthrough curves deviated from ideal adsorption system with an S-shaped profile characteristic. The τ values decreased with increasing flow rate, influent phosphate concentration, pH, and adsorbent particle size, and by decreasing the bed height. Conversely, the k_{YN} values indicated opposite trends in τ values. For instance, increasing the flow rate or decreasing the bed height resulted in an increase in phosphate ions passing the packed adsorbent for a given period of time. Consequently, k_{YN} increased and τ decreased.

The Thomas and MDR models were also applied to the experimental phosphate adsorption curves to depict the entire breakthrough curve. The Thomas model is based on the assumption that adsorption is only controlled by the surface reaction between the adsorbate and adsorbent surface, where the effects of intra-particle diffusion and external film resistances are neglected (Chittoo and Sutherland, 2020). The MDR model was developed based on mathematical issues to reduce the error resulting from the Thomas model (Sana and Jalila, 2017). The values of predicted q_{Th} and q_{mdr} were close to the experimental q values (percentage errors < 3%), except for d values of 0.5–1.0 nm. Additionally, their trends in response to

Table 3: Yoon-Nelson, Thomas, and MDR model parameters for phosphate adsorption by am-Zr/MgFe-LDH composite in fixed-bed column at various experimental conditions

Experimental conditions No.	Yoon-Nelson			Thomas			MDR		
	k_{YN} ($\times 10^{-2}$)	τ	R^2	k_{Th} ($\times 10^{-3}$)	q_{Th}	R^2	q_{mdr}	a	R^2
1	0.96	17.33	0.958	0.76	19.91	0.958	19.94	8.157	0.966
2	1.59	10.65	0.962	1.29	19.02	0.962	19.01	8.583	0.969
3	1.92	7.19	0.984	1.55	18.44	0.984	18.31	7.796	0.990
4	1.82	7.11	0.961	1.01	19.10	0.972	18.79	4.845	0.985
5	0.95	14.48	0.960	0.76	19.49	0.960	19.45	6.987	0.970
6	0.70	22.28	0.974	1.33	17.16	0.974	17.10	8.693	0.981
7	2.19	6.21	0.968	0.81	19.05	0.964	19.05	6.980	0.975
8	0.81	12.83	0.916	0.48	24.67	0.926	24.66	4.418	0.953
9	1.89	8.40	0.974	1.16	15.84	0.978	15.73	6.840	0.986
10	0.52	8.66	0.943	0.42	15.61	0.943	15.33	2.516	0.985
11	0.25	5.78	0.864	0.21	10.21	0.864	10.80	1.370	0.931

various experimental conditions were similar to those of the experimental *q*. However, the Thomas model was not completely fit with the experimental curves as the phosphate adsorption on the am-Zr/MgFe-LDH composite involved intra-particle diffusion as the rate-limiting step. The slow intra-particle diffusion of phosphate on the composite pores was signified by the considerably slow adsorption from the *C*/*Co* ratio of 0.85 to reach 1 (Chu, 2004). As can be seen from Table 3, the MDR model showed larger R^2 values than those of the Yoon-Nelson and Thomas models for all experimental conditions. This indicates that the phosphate adsorption behavior of the packed am-Zr/MgFe-LDH composite in a fixed-bed column system was better described by the MDR model in each experimental condition. As the MDR model based on the Thomas model, the results suggest that adsorption follows the Langmuir isotherm, which suggests that the driving forces obey second-order reversible reaction kinetics with no axial dispersion in the column (Sana and Jalila, 2017).

Phosphate adsorption from real municipal anaerobic sludge filtrate and synthetic seawater

The anaerobic sludge used in this study was collected from an eastern municipal wastewater treatment plant in Ube, Japan. Before use in the column adsorption test, the sludge was allowed to stand for 24 h for deposition, and the supernatant was filtered using a 0.45 µm filter membrane. The effect of seawater ions on phosphate adsorption in seawater was also investigated using synthetic phosphate-containing seawater (P seawater). As 99% of the seawater electrolyte concentration consists of NaCl, Na_2SO_4, KCl, $MgCl_2$, and $CaCl_2$, synthetic seawater was prepared using these salts, corresponding to a salinity of 15 PSU (Zhang *et al*., 2020). The 15 PSU salinity was chosen to represent the salinity of the mesohaline estuary (salinity ranges from 5 to 18 PSU), an area that has great potential to be eutrophic and needs attention (Brush, 2009). For comparison, phosphate adsorption was also conducted in synthetic phosphate-containing water (P water). The details of the sludge, synthetic P seawater, and P water are listed in Table 4. In this experiment, an adsorbent particle size range of 0.1–0.5 mm was used to prevent column clogging by extremely small particles present in the sludge filtrate. Each water sample was pumped through the 1.0 g of adsorbent column at flow rate of 2.5 mL/min.

Fig. 3 shows a comparison of the breakthrough curves for phosphate adsorption onto the composite-packed column using real anaerobic sludge filtrate, synthetic P water, and seawater. The earlier breakthrough of phosphate adsorption in anaerobic sludge might be due to the high concentration of carbonate (CO_3^{2-}), which is signified by high alkalinity (Table 4). Nuryadin *et al*. (2021) found that CO_3^{2-} (or bicarbonate) was highly competitive with phosphate for the active binding sites on the adsorption surface. Furthermore, the presence of extremely fine suspended solids that passed through the filter during filtration in the filtrate could interfere with the transfer of phosphate from the bulk liquid to the am-Zr/MgFe-LDH composite surface (Sun *et al*., 2014). The adsorption capacity of the sludge filtrate (8.99 mg-P/L) was lower than that in synthetic P water (13.12 mg-P/L). However, phosphate adsorption was not negatively affected by the seawater ions, but was enhanced after the breakthrough point passed. The adsorption capacity in synthetic P seawater was 19.99 mg-P/L. The positively charged seawater ions (such as Na^+, Mg^{2+}, Ca^{2+}, and K^+) in the solution were easily attracted by an adsorbent surface that became more

Table 4: The details of anaerobic sludge filtrate, synthetic P water, and synthetic P seawater used in fixed-bed column phosphate adsorption

Anaerobic sludge filtrate		Synthetic P seawater		Synthetic P water	
Parameter	Value	Parameter	Value	Parameter	Value
pH	8.51	pH	8.10	pH	8.51
Phosphate (PO_4-P)	14.24 mg/L	Phosphate (PO_4-P)	14.58 mg/L	Phosphate (PO_4-P)	14.23 mg/L
TSS	168.67 mg/L	NaCl	10519.20 mg/L		
COD	400.00 mg/L	$MgCl_2$	2094.64 mg/L		
Chloride (Cl^-)	574.82 mg/L	Na_2SO_4	1704.48 mg/L		
Nitrate (NO_3^--N)	14.58 mg/L	$CaCl_2$	488.31 mg/L		
Alkalinity ($CaCO_3$)	109.70 mg/L	KCl	298.21 mg/L		

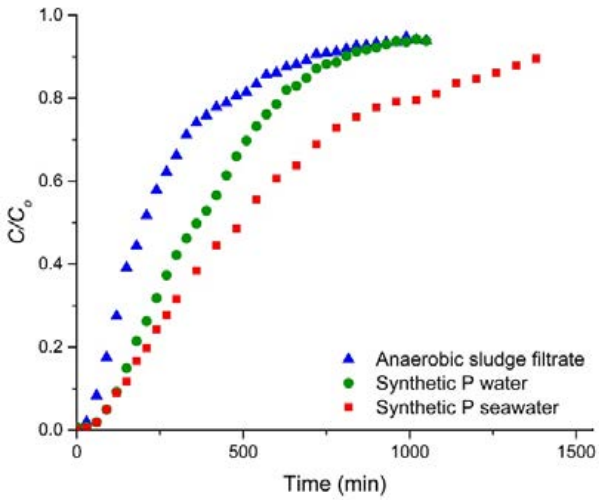


Fig. 3: Breakthrough curves for phosphate adsorption from anaerobic sludge filtrate, synthetic P water, and synthetic P seawater (m = 1.01 g, Q = 2.5 mL/min, d = 0.1-0.5 mm)

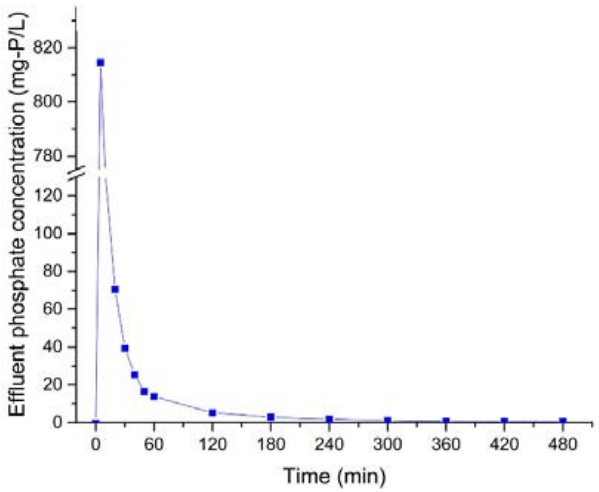


Fig. 4: Continuous phosphate desorption curve on am-Zr/MgFe-LDH composite column by 0.1 N NaOH (h = 1.5 cm and Q = 2.5 mL/min)

negatively charged after initial phosphate adsorption. This increased positive charge on the adsorbent surface and promoted subsequent phosphate adsorption. According to the results, the composite adsorption capacity reduced due to the highly carbonated wastewater in the continuous adsorption system. However, it exhibited more favorable phosphate adsorption in synthetic seawater.

Column regeneration and reusability

The effectiveness of the adsorbent for practical applications depends on the adsorption capacity and efficiency of adsorbent regeneration and reusability. However, the reuse of an adsorbent requires a desorption agent to desorb phosphate from the adsorbent for regeneration. To ensure that the adsorbent was saturated with phosphate before the regeneration study, a phosphate solution (C_o = 12 mg-P/L, pH = 7) was pumped (Q = 2.5 mL/min) to the column (h = 1.5 cm, $d \leq$ 0.1 mm) for 24 h. The exhausted composite was regenerated with 0.1 N NaOH at a flow rate of 2.5 mL/min. The effluent

phosphate concentrations in a continuous desorption curve of phosphate at particular time points were determined and are shown in Fig. 4.

The desorption curve was an asymmetrically shaped curve with significantly high desorption at the beginning, followed by a flattened decline. The regeneration study was conducted for 8 h when the effluent concentration was 0.51 mg-P/L. Fig. 4 shows that the maximum phosphate concentration was obtained within 5–10 min, indicating that the majority of the phosphate amount desorbed during this period. The flattened curve was observed after a one-hour desorption, indicating that almost complete desorption was achieved after 1 h with a desorption efficiency (100 % × $q_{desorbed}/q_{adsorbed}$) of 91.7% and an effluent concentration of 13.82 mg-P/L. However, a total regeneration of 98.8% was achieved after an eight-hour operation. The regenerated column was reused for subsequent adsorption to assess the reusability of the column, and its breakthrough curves and regeneration capacity after eight adsorption-desorption cycles are shown in Fig. 5. A significant decrease in the column adsorption capacity (~8.0%) was observed in the second cycle, as depicted by the earlier breakthrough point after the first cycle (Fig. 5a). These breakthrough points appeared to shift slowly to an earlier time, signifying a slow decrease in the adsorption capacity after the second cycle (Fig. 5b). The gradual decrease in adsorption performance is attributed to the loss of active binding sites from the previous adsorption process, particularly in the first cycle, by strongly attached phosphate, which is difficult to desorb. The decrease in adsorption capacity from the first to the eighth cycle was approximately 17%, indicating that the composite may be suitable for practical applications.

Adsorption mechanism

The possible mechanism of phosphate adsorption by the composite was further investigated using FTIR, XRD, point of zero charge (PZC), and XPS analyses. The functional groups of the composite before and after adsorption were identified using FTIR spectroscopy, and the spectra are shown in Fig. 6a. The intense and broadband centered at 3430 cm^{-1} and the band at 1640 cm^{-1} could be attributed to strong OH stretching and structural OH bending vibrations due to the presence of structural hydroxyl groups and physically adsorbed water molecules in the samples, respectively (Su *et al.*, 2013; Tang *et al.*, 2018). The bands of the Zr-OH bending vibration were observed at approximately 1353 cm^{-1} and 1565 cm^{-1}, and the band of CO_3^{2-} antisymmetric stretching in the interlayer was detected at 1358 cm^{-1} (Dou *et al.*, 2012; Magri *et al.*, 2019; Zhang *et al.*, 2013). These bands were weakened after phosphate adsorption, indicating that phosphate anions were successfully adsorbed by replacing hydroxyl bonds and by exchanging some carbonate anions in the LDH interlayer. In addition, phosphate adsorption

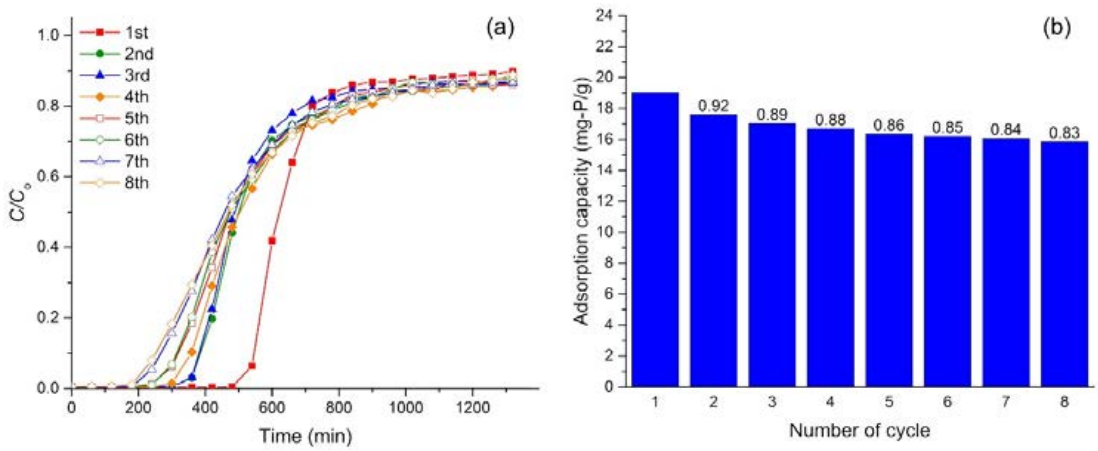


Fig. 5: Column reusability study: (a) phosphate adsorption breakthrough curve on am-Zr/MgFe-LDH composite for each consecutive eight adsorption-desorption cycles at a flow rate 2.5 mL/min, and (b) column adsorption capacity calculated for each adsorption cycle (the numbers above the bar are adsorption retain ratio of phosphate adsorption capacity)

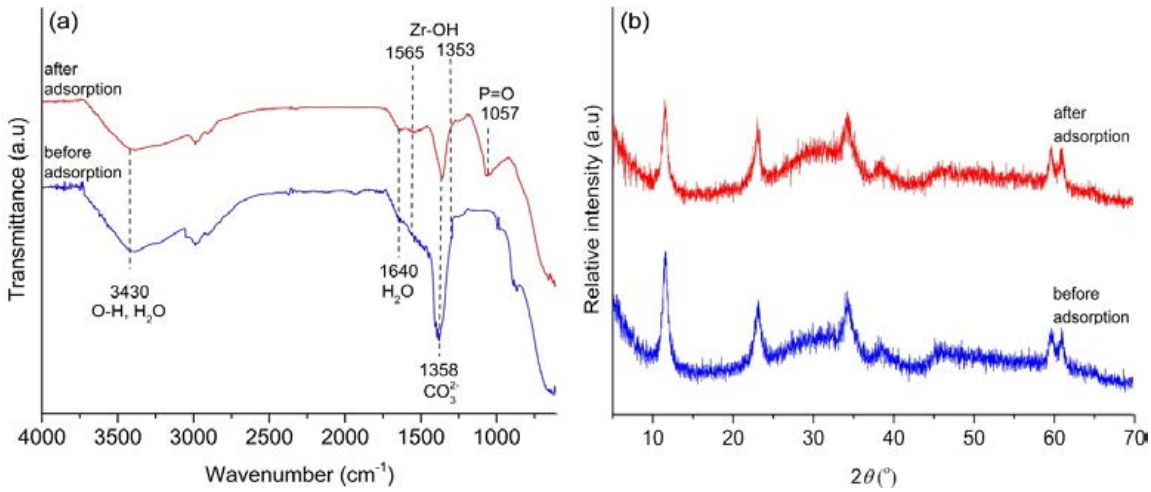


Fig. 6: (a) FTIR spectra and (b) XRD patterns of am-Zr/MgFe-LDH composite before and after adsorption

in the composite was confirmed by the appearance of a new peak near 1057 cm^{-1} after the adsorption process, which could be attributed to the P=O bond (Zha *et al*., 2018).

Fig. 6b shows a comparison between the XRD patterns of the composite, before and after phosphate adsorption. The patterns exhibited the presence of an LDH structure with a typical halo pattern of amorphous zirconium hydroxide. There was no significant change in the structure and no additional characteristic peak was observed in the patterns after the adsorption process. However, the structure showed a lower crystallinity. The decrease in crystallinity confirmed the occurrence of phosphate adsorption, which caused a disordered structure in the composite surface.

The phosphate adsorption mechanism was further evaluated by deconvolution of the XPS spectra. As depicted in Fig. 7a and Fig. 7b, the peaks of the Mg 1s and Fe 2p spectra shifted to higher binding energies after phosphate adsorption by about 0.2 eV for Mg 1s, 0.4 eV for Fe 2p1, and 0.2 eV for Fe 2p3. This enhancement of binding energy values was caused by electron withdrawal from the negatively charged O atoms of the phosphate species to the valence band of Mg s1 and Fe 2p and the formation of Mg-O-P and Fe-O-P through surface complexation (Hong *et al*., 2019; Liu *et al*., 2019). This indicated that the surface of LDH in the composite was also involved in the phosphate adsorption process. As presented in Fig. 7c, the two peaks centered at 181.85 eV and 184.20 eV were assigned to Zr-O-Zr bonds of Zr $3d_{5/2}$ and Zr $3d_{3/2}$ in the composite, respectively. The main peaks of Zr 3d were shifted to a higher binding energy of approximately 0.2 eV after phosphate adsorption, indicating that electron transfer occurred in the valence band and Zr-O-P inner-sphere complexation was formed by substituting the hydroxyl groups of am-Zr (Zhang *et al*., 2019). This shift also can be attributed to the overlap from two new Zr-P peaks in higher binding energies (182.35 eV and 184.79 eV) which formed through ligand exchange (Zong *et al*., 2016). These indicated that phosphate was adsorbed chemically on the composite surface. As shown in Fig. 7d, the C 1s spectra of the composite can be divided into four different peaks: C-C (284.5 eV), C-O (285.2 eV), C=O (288.8 eV), and metal carbonate (M-CO_3) (289.6 eV) (Lai *et al*., 2020). After phosphate adsorption, the relative area of the metal carbonate decreased from 14.7% to 5.2%. This signified that the carbonate in the LDH interlayer took part in the phosphate adsorption process via ion and ligand exchange.

Nuryadin *et al*. (2021) reported that the adsorption was high at low pH (particularly at pH 2 and 3) and decreased at higher pH (notably at pH 10). To explain this condition, the pH_{pzc} of the composite was investigated by PMT, and the plotted experimental curves are shown in Fig. 8. The curves show an intersection point at a pH of approximately 9.7, which

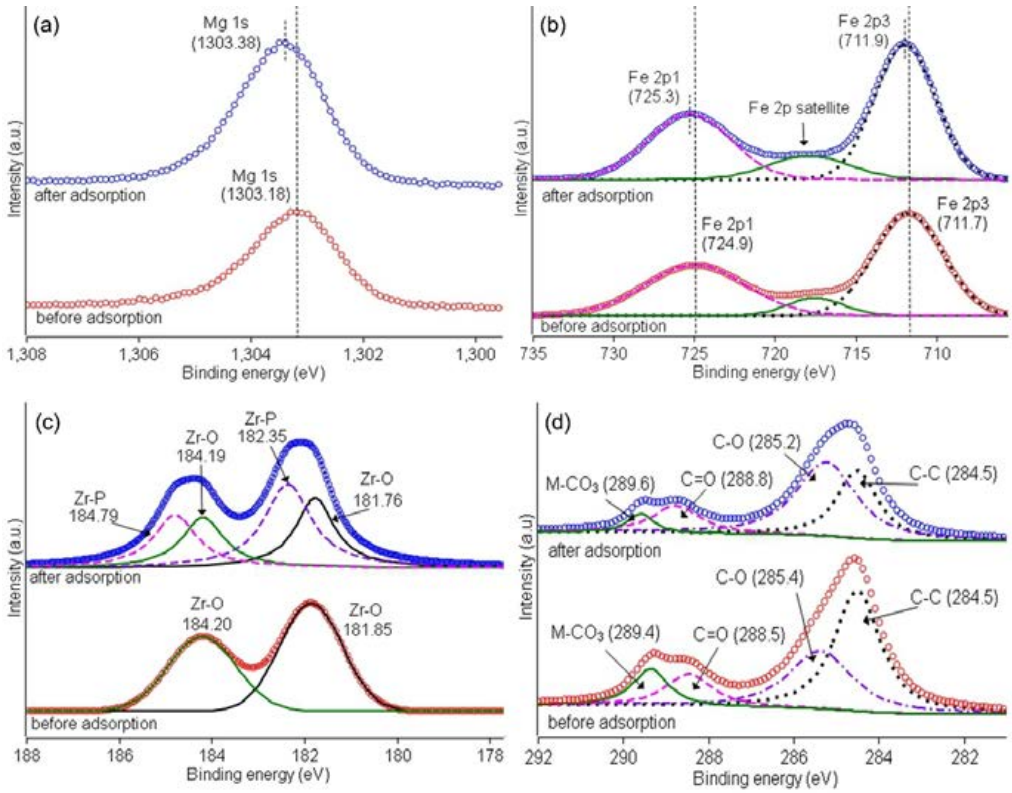


Fig. 7: XPS analysis of am-Zr/MgFe-LDH composite before and after phosphate adsorption: (a) Mg 1s, (b) Fe 2p, (c) Zr 3d, and (d) C 1s

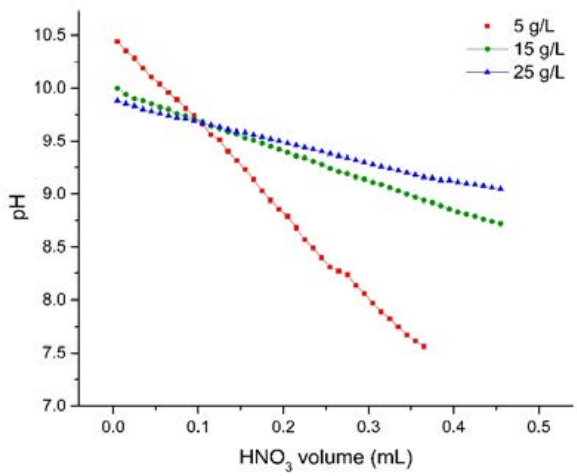


Fig. 8: Potentiometric mass titration curves of am-Zr/MgFe-LDH composite samples using 0.1 M HNO_3

was identified as the pH_{pzc} of the composite. This indicates that the significant decrease in adsorption efficiency at pH 10 was triggered by the negatively charged composite surface as the solution pH was higher than pH_{pzc}. This result indicates that the electrostatic bond also contributed to the phosphate

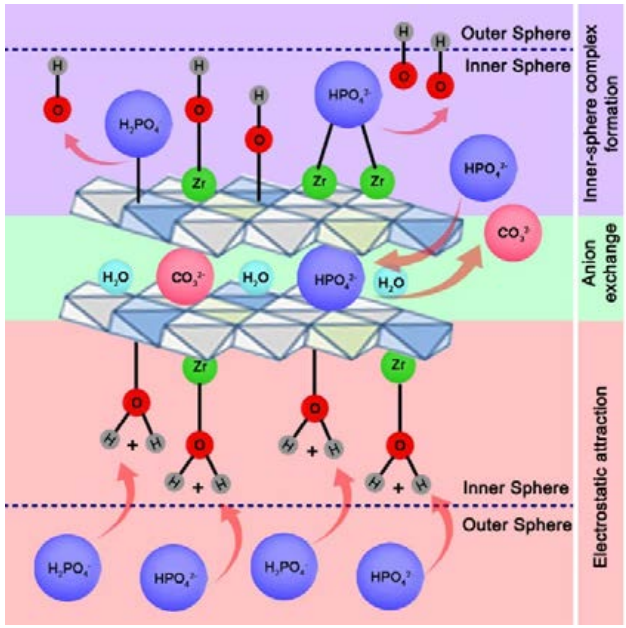


Fig. 9: Proposed mechanism of phosphate adsorption on am-Zr/MgFe-LDH composite

adsorption mechanism between the composite surface and phosphate anions, particularly at pH values lower than 9.7.

Based on the analysis of adsorption in varying pH solutions, FTIR spectra, XRD patterns, and XPS spectra, the potential adsorption mechanisms involved in the composite during the adsorption process were found to mainly consist of electrostatic attraction between the positively charged adsorbent surface and phosphate anions (particularly at low pH), inner-sphere complex formation between metal hydroxides and phosphate anions on the adsorbent surface, and exchange of carbonate anions in the LDH interlayer. The proposed phosphate-adsorption mechanism is illustrated in Fig. 9. The presence of am-Zr on the surface of the LDH likely increased the adsorption capacity of the composite. The zirconium species, which is in amorphous form, have a massive number of hydroxyl groups as the active binding sites for the phosphate anions. Moreover, the crystallization of am-Zr on the LDH matrix was presumably suppressed during synthesis, leading to the formation of nanosized am-Zr (Nuryadin *et al.*, 2021). The nanosized materials are preferable for adsorbent because the crystal has a large surface area for adsorption sites. Therefore, we suggest that the high phosphate adsorption of the composite is mainly associated with the presence of highly hydrated am-Zr collaborated with the ability of MgFe-LDH for adsorbing phosphate by anion exchange and surface adsorption.

CONCLUSION

This study involves the application of a synthesized am-Zr/MgFe-LDH composite as a phosphate sorbent in a continuous fixed-bed column system as well as the investigation of the feasibility of its reusability using NaOH solution in regeneration process. The results of the column experiments showed that the phosphate adsorption capacity of the composite was affected by the flow rate, bed height, influent phosphate concentration, influent pH, and composite particle size. The increase in the flow rate, pH, and adsorbent particle size, decreased the phosphate adsorption capacity of the composite. Contrarily, the phosphate adsorption capacity of the composite increased with increasing bed height and influent phosphate concentration in the fixed-bed column system. The highest adsorption capacity of 25.15 mg-P/L was obtained when the influent pH was 4, indicating that the adsorption of phosphate onto the composite surface is favorable in acidic. From the

non-linear fitting of the breakthrough data, the MDR model was found to be the best model for predicting the experimental phosphate adsorption behavior of a packed composite in a fixed-bed column system, as compared to the Yoon-Nelson and Thomas models. The phosphate adsorption capacity of the composite decreased when it was used in wastewater with a high (bi)carbonate concentration. However, it exhibited a more effective phosphate adsorption in synthetic seawater. The column regeneration studies revealed that 91.7 % of adsorbed phosphorus was desorbed during the one-hour desorption, and 83% of the fresh composite adsorption ability could be retained even after eight adsorption-desorption cycles. The pH_{pzc}, FTIR, XRD, and XPS analyses indicated that electrostatic attraction, inner-sphere complexation, and anion exchange played an important role in phosphate adsorption. The am-Zr/MgFe-DH composite has the potential to be utilized as an adsorbent for phosphorus removal from aqueous solutions as it has high phosphate adsorption capacity and reusability. Although, this study provides helpful information for the design of a practical system for phosphorus removal and recovery, some considerations should be taken to improve the performance of the composite adsorption system in future work. First, the application of economical pretreatment to reduce (bi)carbonate from wastewater before process, such as chemical precipitation, since (bi)carbonate is the most competitive anion for phosphate adsorption onto the composite. Second, the use of adsorption byproduct to create an economic adsorption system, such as the processing of desorbed phosphorus in the regeneration process to a valuable product like hydroxyapatite, or the application of saturated composite as the slow release phosphate fertilizer.

AUTHOR CONTRIBUTIONS

A. Nuryadin performed the literature review, conception and design, acquisition of data, analysis and interpretation of data, drafting of the manuscript, and statistical analysis. T. Imai performed conception and design, critical revision of the manuscript for important intellectual content, supervision, and support for administrative, technical, and material.

ACKNOWLEDGEMENT

A. Nuryadin expresses his gratitude to the support of the Indonesian Ministry of Research, Technology, and Higher Education (RISTEK-DIKTI), as well as the Project Implementation Unit (PIU) of the Islamic Development Bank (IsDB) 4in1 Project of Mulawarman University for providing the scholarship. The authors would also like to thank T. Suzuki for assistance with FTIR analysis and Editage for English language editing.

CONFLICT OF INTEREST

The authors declare no potential conflict of interest regarding the publication of this work. In addition, the ethical issues including plagiarism, informed consent, misconduct, data fabrication and, or falsification, double publication and, or submission, and redundancy have been completely witnessed by the authors.

ABBREVIATIONS

a	A modified dose-response model parameter
A-Zr-NP	Alginate-/Zirconium-Grafted Newspaper Pellets
am-Zr	amorphous zirconium (hydr)oxide
am-Zr/MgFe-LDH	amorphous zirconium (hydr)oxide/ MgFe layered double hydroxides
C	Carbon
C	Effluent concentration
C_o	Influent concentration
Ca^{2+}	Calcium ion
$CaCl_2$	Calcium chloride
$CaCO_3$	Calcium carbonate
Cl^-	Chloride ion
cm	Centimeter
CO_3^{2-}	Carbonate ion
COD	Chemical oxygen demand
CS-Zr-PEPA	Polyethyene polyamine grafted chitosan-zirconium(IV) composite beads
Cu-Kα	Copper K-alpha
d	Particle size
DI	Deionized
EAP	Eluted amount of phosphorus
eV	Electron volt
Fe	Iron
$FeCl_3{\cdot}6H_2O$	Iron(III) chloride hexahydrate
FTIR	Fourier transform infrared
g	Gram

h	Hour
h	Bed height
HCl	Hydrochloric acid
HNO_3	Nitric acid
K	Kelvin
K^+	Potassium ion
K_2HPO_4	Dipotassium hydrogen phosphate
KCl	Potassium chloride
KNO_3	Potassium nitrate
KOH	Potassium hydroxide
k_{Th}	Thomas kinetic coefficient
kV	Kilovolt
K_{YN}	Yoon-Nelson kinetic coefficient
L	Liter
LDH	Layered double hydroxides
M	Molar
m	Mass
MDR	Modified dose-response
Mg	Magnesium
mg	milligram
mg-P	Milligram as phosphorus
Mg^{2+}	Magnesium ion
$MgCl_2$	Magnesium chloride
$MgCl_2{\cdot}6H_2O$	Magnesium chloride hexahydrate
MgFe-LDH	Magnesium iron layered double hydroxides
min	Minute
mL	Milliliter
mm	Millimeter
N	Normal
N_2	Nitrogen
n2	Number of the last fraction in the desorption operation
Na^+	Natrium ion
Na_2CO_3	Sodium carbonate
Na_2SO_4	Sodium sulfate
NaCl	Sodium chloride
NaOH	Sodium Hydroxide
nm	Nanometer
NO_3^--*N*	Nitrate as nitrogen
O	Oxygen
OH	Hydroxyl
OH^-	Hydroxyl ion
P	Phosphorus
P seawater	Synthetic phosphate-containing seawater
P water	Synthetic phosphate-containing water
PAOs	polyphosphate-accumulating organisms
pH_{pzc}	pH at the point of zero charge
PMT	Potentiometric mass titration
PO_4-*P*	Phosphate as phosphorus
PSU	Practical salinity unit
PZC	Point of zero charge
Q	Flow rate
$q_{adsorbed}$	Total amount of adsorbed phosphate
$q_{desorbed}$	Total amount of desorbed phosphate
q_e	Equilibrium adsorption capacity
Q_{mdr}	Predicted adsorption capacity of modified dose-response model
q_{th}	Predicted adsorption capacity of Thomas model
R^2	Coefficient of determination
rpm	Rotation per minute
t	Time
t_b	Breakthrough time
t_e	Time required to reach exhaustion time
TSS	Total suspended solid
V_q	Effluent volume of the *q* -th fraction
XPS	X-ray photoelectron spectroscopy
XRD	X-ray diffraction
Zr	Zirconium
Zr(IV)-loaded okara	Soybean residue (okara) loaded with zirconium(IV)
Zr(IV)-loaded SOW gel	Saponified orange waste gel loaded with zirconium(IV)
Zr-FPS	Fiber containing phosphonate and sulfonate (FPS) loaded with zirconium(IV)
$ZrOCl_2{\cdot}8H_2O$	Zirconyl chloride octahydrate
µm	Micrometer
τ	Time required for 50% adsorption breakthrough
%	Percent

REFERENCES

Awual, M.R.; Jyo, A.; Ihara, T.; Seko, N.; Tamada, M.; Lim, K.T., (2011). Enhanced trace phosphate removal from water by zirconium(IV) loaded fibrous adsorbent. Water Res., 45:4592–4600 **(9 pages)**.

Biswas, B.K.; Inoue, K.; Ghimire, K.N.; Harada, H.; Ohto, K.; Kawakita, H., (2008). Removal and recovery of phosphorus from water by means of adsorption onto orange waste gel loaded with zirconium. Bioresour. Technol., 99:8685–8690 **(6 pages)**.

Bourikas, K.; Vakros, J.; Kordulis, C.; Lycourghiotis, A., (2003). Potentiometric mass titrations: Experimental and theoretical establishment of a new technique for determining the point of zero charge (PZC) of metal (Hydr)Oxides. J. Phys. Chem. B., 107(35): 9441–9451 **(11 pages)**.

Brush, G.S., (2009). Historical Land Use, Nitrogen, and Coastal Eutrophication: A Paleoecological Perspective. Estuaries Coasts., 32(1):18-28 **(11 pages)**.

Chen, Z.; Luo, H.; Rong, H., (2020). Development of polyaminated chitosan-zirconium(IV) complex bead adsorbent for highly efficient removal and recovery of phosphorus in aqueous solutions. Int. J. Biol. Macromol., 164:1183–1193 **(11 pages)**.

Chittoo, B.S.; Sutherland, C., (2020). Column breakthrough studies for the removal and recovery of phosphate by lime-iron sludge: Modeling and optimization using artificial neural network and adaptive neuro-fuzzy inference system. Chinese J. Chem. Eng., 28(7):1847-1859 **(13 pages)**.

Chu, K.H., (2004). Improved fixed bed models for metal biosorption. Chem. Eng. J., 97(2-3):233-239 **(7 pages)**.

Dash, S.; Borah, S.S.; Kalamdhad, A.S., (2020). Study of the limnology of wetlands through a one-dimensional model for assessing the eutrophication levels induced by various pollution sources. Ecol. Modell., 416:108907 **(15 pages)**.

Dou, X.; Mohan, D.; Pittman, C.U.; Yang, S., (2012). Remediating fluoride from water using hydrous zirconium oxide. Chem. Eng. J., 198-199:236-245 **(10 pages)**.

Gouran-Orimi, R.; Mirzayi, B.; Nematollahzadeh, A.; Tardast, A., (2018). Competitive adsorption of nitrate in fixed-bed column packed with bio-inspired polydopamine coated zeolite. J. Environ. Chem. Eng., 6(2):2232-2240 **(9 pages)**.

He, Y.; Lin, H.; Dong, Y.; Liu, Q.; Wang, L., (2016). Simultaneous removal of phosphate and ammonium using salt–thermal-activated and lanthanum-doped zeolite: fixed-bed column and mechanism study. Desalin. Water Treat., 57(56):27279-27293 **(15 pages)**.

Hong, X.; Zhu, E.; Ye, Z.; Hui, K.S.; Hui, K.N., (2019). Enhanced phosphate removal under an electric field via multiple mechanisms on MgAl-LDHs/AC composite electrode. J. Electroanal. Chem., 836:16-23 **(8 pages)**.

Husein, D.Z.; Al-Radadi, T.; Danish, E.Y., (2017). Adsorption of phosphate using alginate-/zirconium-grafted newspaper pellets: fixed-bed column study and application. Arab. J. Sci. Eng., 42:1399–1412 **(14 pages)**.

Jiang, D.; Chu, B.; Amano, Y.; Machida, M., (2018). Removal and recovery of phosphate from water by Mg-laden biochar: Batch and column studies. Colloids Surfaces A Physicochem. Eng. Asp. 558:429-437 **(9 pages)**.

Kumar, P.S.; Korving, L.; van Loosdrecht, M.C.M.; Witkamp, G.J., (2019). Adsorption as a technology to achieve ultra-low concentrations of phosphate: Research gaps and economic analysis. Water Res. X. 4:100029 **(17 pages)**.

Kumar, R.; Bhatia, D.; Singh, R.; Rani, S.; Bishnoi, N.R., (2011). Sorption of heavy metals from electroplating effluent using immobilized biomass Trichoderma viride in a continuous packed-bed column. Int. Biodeterior. Biodegradation. 65(8):1133-1139 **(7 pages)**.

Lai, Y.T.; Huang, Y.S.; Chen, C.H.; Lin, Y.C.; Jeng, H.T.; Chang, M.C.; Chen, L.J.; Lee, C.Y.; Hsu, P.C.; Tai, N.H., (2020). Green treatment of phosphate from wastewater using a porous bio-templated graphene oxide/MgMn-layered double hydroxide composite. iScience. 23(5):101065 **(24 pages)**.

Lee, S.Y.; Choi, J.W.; Song, K.G.; Choi, K.; Lee, Y.J.; Jung, K-W., (2019). Adsorption and mechanistic study for phosphate removal by rice husk-derived biochar functionalized with Mg/Al-calcined layered double hydroxides via co-pyrolysis. Compos. Part B Eng., 176:107209 **(15 pages)**.

Liu, R.; Chi, L.; Wang, X.; Wang, Y.; Sui, Y.; Xie, T.; Arandiyan, H., (2019). Effective and selective adsorption of phosphate from aqueous solution via trivalent-metals-based amino-MIL-101 MOFs. Chem. Eng. J., 357:159-168 **(10 pages)**.

Magri, V.R.; Duarte, A.; Perotti, G.F.; Constantino, V.R.L., (2019). Investigation of thermal behavior of layered double hydroxides intercalated with carboxymethylcellulose aiming bio-carbon based nanocomposites. Chem. Eng., 3(2):55 **(17 pages)**.

March, M.D.; Toma, L.; Stott, A.W.; Roberts, D.J., (2016). Modelling phosphorus efficiency within diverse dairy farming systems – pollutant and non-renewable resource?. Ecol. Indic., 69:667-676 **(10 pages)**.

Marzbali, M.H.; Esmaieli, M., (2017). Fixed bed adsorption of tetracycline on a mesoporous activated carbon: Experimental study and neuro-fuzzy modeling. J. Appl. Res. Technol., 15(5):454-463 **(10 pages)**.

Mohan, R.; Dutta, R.K., (2020). Continuous fixed-bed column assessment for defluoridation of water using HAp-coated-limestone. J. Environ. Chem. Eng., 8(4):103840 **(9 pages)**.

Nguyen, T.A.H.; Ngo, H.H.; Guo, W.S.; Pham, T.Q.; Li, F.M.; Nguyen, T.V.; Bui, X.T., (2015). Adsorption of phosphate from aqueous solutions and sewage using zirconium loaded okara (ZLO): Fixed-bed column study. Sci. Total Environ. 523:40-49 **(10 pages)**.

Nuryadin, A.; Imai, T.; Kanno, A.; Yamamoto, K.; Sekine, M.; Higuchi, T., (2021). Phosphate adsorption and desorption on two-stage synthesized amorphous-ZrO2/Mg-Fe layered double hydroxide composite. Mater. Chem. Phys., 266:124559 **(10 pages)**.

Oguz, E., (2017). Fixed-bed column studies on the removal of Fe3+ and neural network modelling. Arab J. Chem., 10(3):313-320 **(8 pages)**.

Ramasahayam, S.K.; Guzman, L.; Gunawan, G.; Viswanathan, T., (2014). A comprehensive review of phosphorus removal technologies and processes. J. Macromol. Sci. Part A., 51(6):538-545 **(8 pages)**.

Sana, D.; Jalila, S., (2017). A comparative study of adsorption and regeneration with different agricultural wastes as adsorbents for the removal of methylene blue from aqueous solution. Chinese J. Chem. Eng., 25(9):1282-1287 **(6 pages)**.

Sotelo, J.L.; Ovejero, G.; Rodríguez, A.; Álvarez, S.; García, J., (2012). Removal of atenolol and isoproturon in aqueous solutions by adsorption in a fixed-bed column. Ind. Eng. Chem. Res., 51(13):5045-5055 **(11 pages)**.

Su, Y.; Cui, H.; Li, Q.; Gao, S.; Shang, J.K., (2013). Strong adsorption

of phosphate by amorphous zirconium oxide nanoparticles. Water Res., 47(14):5018-5026 **(9 pages)**.

Sun, X.; Imai, T.; Sekine, M.; Higuchi, T.; Yamamoto, K.; Kanno, A.; Nakazono, S., (2014). Adsorption of phosphate using calcined Mg3–Fe layered double hydroxides in a fixed-bed column study. J. Ind. Eng. Chem., 20(5):3623-3630 **(8 pages).**

Taka, A.L.; Klink, M.J.; Mbianda, X.Y.; Naidoo, E.B., (2020). Chitosan nanocomposites for water treatment by fixed-bed continuous flow column adsorption: a review. Carbohydr. Polym. 255:117398 **(15 pages)**.

Tang, N.; He, T.; Liu, J., Li, L.; Shi, H.; Cen, W.; Ye, Z., (2018). New insights into co2 adsorption on layered double hydroxide (LDH)-based nanomaterials. Nanoscale Res. Lett., 13:55 **(7 pages)**.

Thomas, H.C., (1944). Heterogeneous ion exchange in a flowing system. J. Am. Chem. Soc., 66(10):1664-1666 **(3 pages)**.

Wang, X.; Miao, J.; You, S.; Ren, N., (2021). Statistical entropy analysis as a proxy method for quantitative evaluation of phosphorus of a food-based bioethanol system. Resour. Conserv. Recycl., 164:105125 **(9 pages)**.

Yan, G.; Viraraghavan, T.; Chen, M., (2001). A new model for heavy metal removal in a biosorption column. Adsorpt. Sci. Technol., 19(1):25-43 **(19 pages)**.

Yoon, Y.H.; Nelson, J.H., (1984). Application of Gas Adsorption Kinetics I. A theoretical model for respirator cartridge service life. Am. Ind. Hyg. Assoc. J., 45(8):509-516 **(8 pages)**.

Zha, Z.; Ren, Y.; Wang, S.; Qian, Z.; Yang, L.; Cheng, P.; Han, Y.; Wang, M., (2018). Phosphate adsorption onto thermally dehydrated aluminate cement granules. RSC Adv., 8(34):19326-19334 **(9 pages)**.

Zhang, H.; Elskens, M.; Chen, G.; Snoeck, C.; Chou, L., (2020). Influence of seawater ions on phosphate adsorption at the surface of hydrous ferric oxide (HFO). Sci. Total Environ., 721:137826 **(8 pages)**.

Zhang, L.; Wang, Z.; Xu, X.; Chen, C.; Gao, B.; Xiao, X., (2019). Insights into the phosphate adsorption behavior onto 3D self-assembled cellulose/graphene hybrid nanomaterials embedded with bimetallic hydroxides. Sci. Total Environ., 653:897-907 **(11 pages)**.

Zhang, Q.; Du, Q.; Jiao, T.; Pan, B.; Zhang, Z.; Sun, Q.; Wang, S.; Wang, T.; Gao, F., (2013). Selective removal of phosphate in waters using a novel of cation adsorbent: zirconium phosphate (ZrP) behavior and mechanism. Chem. Eng. J., 221:315-321 **(7 pages)**.

Zong, E.; Liu, X.; Jiang, J.; Fu, S.; Chu, F., (2016). Preparation and characterization of zirconia-loaded lignocellulosic butanol residue as a biosorbent for phosphate removal from aqueous solution. Appl. Surf. Sci., 387:419-430 **(12 pages)**.

Zou, Y.; Zhang, R.; Wang, L.; Xue, K.; Chen, J., (2020). Strong adsorption of phosphate from aqueous solution by zirconium-loaded Ca-montmorillonite. Appl. Clay. Sci. 192:105638 **(10 pages)**.

AUTHOR (S) BIOSKETCHES

Nuryadin, A., Ph.D. Candidate, Graduate School of Sciences and Technology for Innovation, Yamaguchi University, Yamaguchi, Japan. Department of Physics Education, Mulawarman University, Samarinda, 75123, Indonesia. Email: *atinnuryadin@hotmail.com*

Imai, T., Ph.D., Professor, Graduate School of Sciences and Technology for Innovation, Yamaguchi University, Yamaguchi, Japan.

Email: *imai@yamaguchi-u.ac.jp*

COPYRIGHTS

©2021 The author(s). This is an open access article distributed under the terms of the Creative Commons Attribution (CC BY 4.0), which permits unrestricted use, distribution, and reproduction in any medium, as long as the original authors and source are cited. No permission is required from the authors or the publishers.

HOW TO CITE THIS ARTICLE

Nuryadin, A.; Imai, T., (2021). Application of amorphous zirconium (hydr)oxide/MgFe layered double hydroxides composite for phosphate removal from water. Global J. Environ. Sci. Manage., 7(4): 485-502.

DOI: 10.22034/gjesm.2021.04.01

url: https://www.gjesm.net/article_243376.html